Our results show that the presence of the female-specific *tra* and the *tra-2* products promote female-specific splicing of *dsx* pre-mRNA and that the 13-nt sequences in the female exon and the female-specific acceptor sequence participate in regulation of *dsx* expression. The *tra* and *tra-2* products may interact directly with the 13-nt sequences in the female-specific exon, and such interactions may allow the suboptimal female-specific polypyrimidine stretch to be recognized as a splicing signal, thus resulting in enhancement of the use of the female-specific acceptor site.

REFERENCES AND NOTES

1. R. Nothiger and M. Steinmann-Zwicky, *Trends Genet.* **1**, 209 (1985); T. W. Cline, in *Origin and Evolution of Sex*, H. O. Halvorson and A. Monroy, Eds. (Liss, New York, 1985), pp. 301–327; B. S. Baker, *Nature* **340**, 521 (1989).
2. B. S. Baker and K. A. Ridge, *Genetics* **94**, 383 (1980).
3. B. S. Baker and M. F. Wolfner, *Genes Dev.* **2**, 477 (1988); K. C. Burtis and B. S. Baker, *Cell* **56**, 997 (1989).
4. R. N. Nagoshi, M. McKeown, K. C. Burtis, J. M. Belote, B. S. Baker, *Cell* **53**, 229 (1988).
5. M. McKeown, J. M. Belote, R. T. Boggs, *ibid.*, p. 887; B. A. Sosnowski, J. M. Belote, M. McKeown, *ibid.* **58**, 449 (1989).
6. K. Inoue, K. Hoshijima, H. Sakamoto, Y. Shimura, *Nature* **344**, 461 (1990).
7. T. Schupbach, *Dev. Biol.* **89**, 117 (1982); J. M. Belote and B. S. Baker, *Proc. Natl. Acad. Sci. U.S.A.* **79**, 1568 (1982); *Dev. Biol.* **95**, 512 (1983).
8. H. Amrein, M. Gorman, R. Nothiger, *Cell* **55**, 1025 (1988); T. J. Goralski, J.-E. Edstrom, B. S. Baker, *ibid.* **56**, 1011 (1989).
9. C. C. Query, R. C. Bentley, J. D. Keene, *ibid.* **57**, 89 (1989); I. W. Mattaj, *ibid.*, p. 1.
10. J. M. Belote, M. McKeown, R. T. Boggs, R. Ohkawa, B. A. Sosnowski, *Dev. Genet.* **10**, 143 (1989).
11. The region from and including the entire third exon to the Pvu II site located 1284 bp downstream of the female acceptor site, and the region from the Acc I site located 250 bp upstream of the male acceptor site to the site located 64 bp downstream of the donor site of the fifth exon, were joined and inserted into the copia vector.
12. M. McKeown, J. M. Belote, R. T. Boggs, *Cell* **53**, 887 (1988).
13. K. Hoshijima *et al.*, unpublished observations.
14. R. N. Nagoshi and B. S. Baker, *Genes Dev.* **4**, 89 (1990).
15. The *dsx* fragment that extends from the third exon to 1128 bp downstream of the female acceptor site and which excludes the polyadenylation signal (Af) was fused to the *ftz* fragment that contains a portion of the intron and the following second exon {corresponding to bases 825 to 2534 of the published sequence [A. Laughon and M. P. Scott, *Nature* **310**, 25 (1984)]}. The resulting fragment was inserted into the copia vector.
16. The region from the third exon (138 bp) to the site 48 bp downstream of the donor site of the third exon, and the region from the site 250 bp upstream of the male acceptor site to the site 64 bp downstream of the donor site of the fifth exon, were joined and inserted into the copia vector.
17. The copia-dsx deletion mutants were constructed as follows: the regions between 345 to 460 bp (R1·5·6), 234 to 459 bp (R5·6), 190 to 480 bp (R6), 344 to 599 bp (R1), or 234 to 599 bp (R0) downstream of the female acceptor site were deleted from copia-dsx, and Kpn I linkers were inserted. A polymerase chain reaction (PCR) fragment that contained the region 268 to 627 bp downstream of the female-specific acceptor site was inserted at the Kpn I linker of the R0 construct in the correct orientation (SR) or in the opposite orientation (ASR). PCR was performed essentially as described [R. K. Saiki *et al.*, *Science* **239**, 487 (1988)].
18. M. R. Green, *Annu. Rev. Genet.* **20**, 671 (1986).
19. Oligonucleotide-directed mutagenesis was performed essentially as described [M. J. Zoller and M. Smith, *Methods Enzymol.* **100**, 468 (1983)].
20. The region 340 to 1128 bp downstream of the female acceptor site was deleted from copia-dtz, copia-dtz(Py18), and copia-dtz(Py13). Pre-mRNA expressed from the deletion construct of copia-dtz was spliced at the *ftz* acceptor site even in the presence of the *tra* and *tra-2* products in Kc cells.
21. We thank M. McKeown for *tra* cDNA and H. Amrein for *tra-2* cDNA. Supported by Grant-in-Aid 62065009 for specially promoted research from the Ministry of Education, Science and Culture of Japan.

1 November 1990; accepted 1 March 1991

Solution Structure of FKBP, a Rotamase Enzyme and Receptor for FK506 and Rapamycin

STEPHEN W. MICHNICK, MICHAEL K. ROSEN, THOMAS J. WANDLESS, MARTIN KARPLUS,* STUART L. SCHREIBER*

Immunophilins, when complexed to immunosuppressive ligands, appear to inhibit signal transduction pathways that result in exocytosis and transcription. The solution structure of one of these, the human FK506 and rapamycin binding protein (FKBP), has been determined by nuclear magnetic resonance (NMR). FKBP has a previously unobserved antiparallel β-sheet folding topology that results in a novel loop crossing and produces a large cavity lined by a conserved array of aromatic residues; this cavity serves as the rotamase active site and drug-binding pocket. There are other significant structural features (such as a protruding positively charged loop and an apparently flexible loop) that may be involved in the biological activity of FKBP.

FKBP IS A SOLUBLE, CYTOSOLIC RE-ceptor (*1, 2*) for the immunosuppressants FK506 and rapamycin (*3*). Both FKBP and cyclophilin (*4–6*), which is a receptor for the immunosuppressant cyclosporin A (CsA), catalyze the interconversion of cis- and trans-rotamers of the peptidyl-prolyl amide bond of peptide and protein substrates. These rotamases are inhibited by their respective immunosuppressive ligands. Mechanistic studies suggest that a complex of immunophilin (immunosuppressant binding protein) and ligand interferes with the intracellular transport of proteins involved in signal transduction pathways associated with both exocytosis (*7*) and transcription (*3, 8*).

In this report we present the solution structure of human FKBP obtained by nuclear Overhauser effect (NOE)–restrained molecular dynamics (rMD) simulations (*9*). The NMR structures satisfying the NOE and empirical energy function restraints have backbone root-mean-square deviations (RMSDs) from the refined average structure in the range of 0.80 to 1.4 Å for the β strands, 0.19 to 0.40 Å for the α helix, and 1.02 Å to 1.72 Å for all residues except 83 to 90 (see below). Many side chains, particularly aromatics, are well defined. FKBP has a novel folding topology in that two loops that connect the strands of an antiparallel β sheet cross one another. Hydrophobic side

chains in the core of the protein form a large, deep pocket that includes the rotamase active site and the drug-binding site. The structure of the binding site appears to be highly conserved in related FK506- and rapamycin-binding proteins.

Sequence-specific assignments of 92% of the observable ^{1}H resonances in FKBP have been made by use of a combination of homonuclear and heteronuclear two-dimensional NMR techniques as reported earlier (*10*). Structural restraints for the dynamics simulations were obtained through empirical calibration of cross-peak magnitudes in nuclear Overhauser effect spectroscopy (NOESY) spectra recorded with mixing times
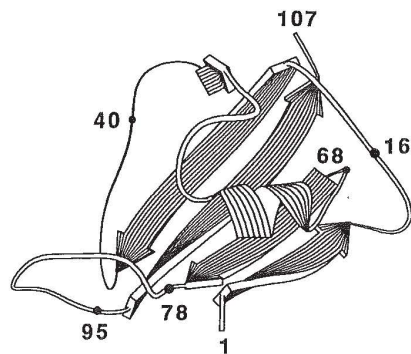

Fig. 1. α-Carbon ribbon drawing of human FKBP; the five-stranded β sheet, α helix, and connecting loops are indicated, as well as the COOH- and NH$_2$-termini and certain residues of interest.

Department of Chemistry, Harvard University, Cambridge, MA 02138.

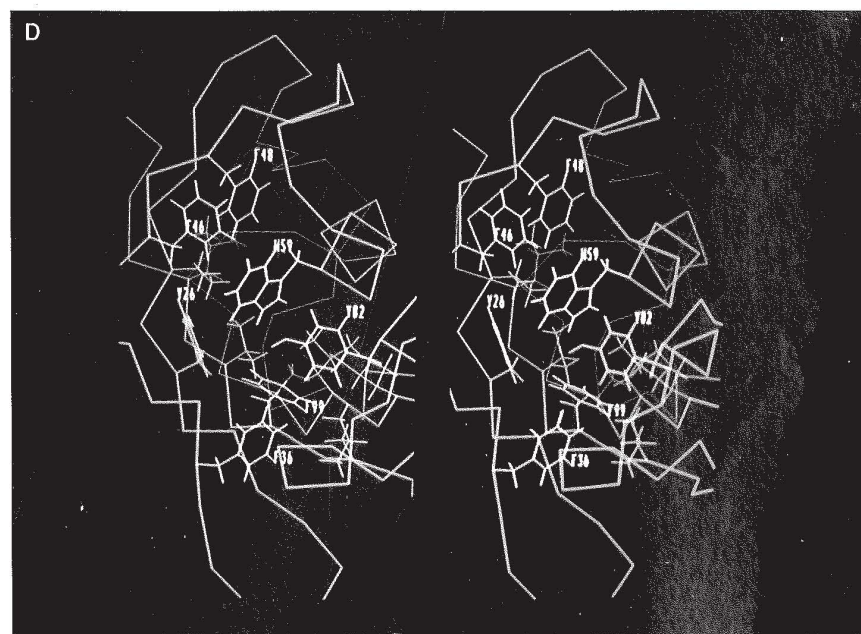*To whom correspondence should be addressed.
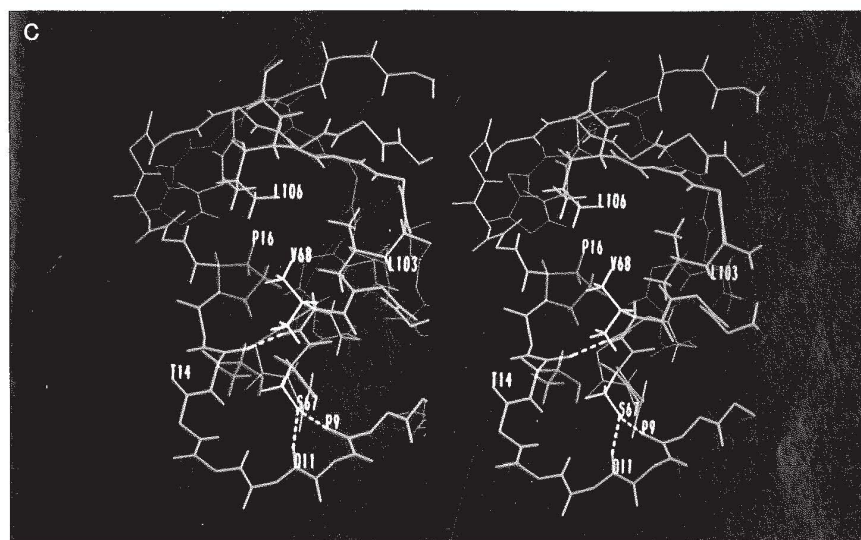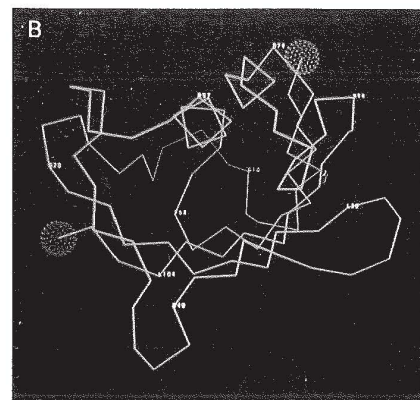
Fig. 2. (**A**) The α-carbon traces of 13 structures generated by restrained molecular dynamics are shown in blue. ⟨SA⟩$_{ref}$, which includes side chains of aromatic residues in the drug-binding pocket, is shown as the heavy line. Aromatic side chains are color-coded: Trp, yellow; Phe, orange; and Tyr, green. The NH$_2$- and COOH-termini are indicated with green and red dot surfaces, respectively. (**B**) ⟨SA⟩$_{ref}$, showing location of the ligand binding site formed by the β sheet and the α helix; certain residues are numbered. (**C**) Expanded view of ⟨SA⟩$_{ref}$, showing crossing of the loops connecting the first and fourth (relevant residues in orange) and the fifth and second (relevant residues in yellow) strands of the β sheet; known interstrand hydrogen bonds are indicated. Relevant residues in the third strand are shown in green. (**D**) Hydrophobic residues in the drug-binding pocket of ⟨SA⟩$_{ref}$. Side chains are color-coded as in (A), with additional aliphatic residues in purple.

of 50, 100, 150, and 200 ms versus known distances in regular secondary structural elements (11). Of particular use in unambiguously determining long-range NOEs were two FKBP samples biosynthetically deuterated at the methyl protons of Leu and Ile and of Val and Ile (12, 13). A total of 860 NOE-derived distance constraints was used in the simulations. In addition, 43 χ_1 dihedral angle restraints (in the range ±60° or ±120°) and 44 backbone ϕ angle restraints (in the range ±60°, ±50°, or ±40°) were used; the angle constraints are based on analysis of coupling constants and cross-peak magnitudes measured in correlated spectroscopy (COSY) spectra, and on NOE data (14). In 32 cases, χ_1 could be restricted to a ±60° range, allowing stereospecific assignment of side chain protons based on intraresidue NOEs from NH and CαH. Hydrogen bond constraints were used for 25 slowly exchanging amide protons. Seventy-nine NOEs, six hydrogen bonds, and six backbone dihedral angles were determined in an iterative manner based on unrefined, restrained structures. The rMD simulations were carried out by using a simulated annealing protocol with the program X-PLOR (9). Statistics indicative of the accuracy and precision of the experimentally determined structure of FKBP and a description of the proto-

col used to generate these structures are provided in Table 1.

The solution structure of FKBP (Figs. 1 and 2) is characterized by a large amphiphilic, antiparallel five-stranded β sheet with +3, +1, −3, +1 topology (15). The strands of the sheet are composed of residues 1 to 7, 20 to 29, 46 to 49, 71 to 77, and 96 to 107. An amphiphilic α helix, formed from residues 59 to 65, packs against the hydrophobic face of the sheet at an angle of 60° with respect to the long axis. The helix is tethered to the fifth and second strands of the sheet by nine- and five-residue loops, respectively. The sheet has a right-handed twist and wraps around the helix to form a well-ordered hydrophobic core (Fig. 1); this structure is in accord with a large number of long-range side chain NOE interactions. Backbone hydrogen-bond propensities are satisfied for the β sheet by interstrand amide-carbonyl contacts and for the α helix by interresidue amide-carbonyl i, $i+3$ contacts. There are no side chain hydrogen bonds between the helix and the sheet, indicating stabilization of these structures through hydrophobic (van der Waals) interactions. The loops connecting the β strands contain secondary structural elements (including several β turns) that satisfy some of the backbone hydrogen bond propensities. The loops are well defined by medium- and long-range NOE contacts except for two regions, residues 37 to 43 and 83 to 90 (see Fig. 2, A and B).

A notable feature of FKBP resulting from the +3, +1, −3, +1 topology of the β sheet is a topological crossing of the loops Ser[8]-Gly[19] and Leu[50]-Gln[70]. A view of this region of the protein is shown in Fig. 2C. Although crossing topologies have been observed in proteins containing parallel β sheets (16), they were presumed to be forbidden in antiparallel sheets (17). The absence of loop crossings has been attributed to the difficulties of obtaining efficient side chain packing, of satisfying the hydrogen bond propensities of the backbone amides of both segments, and of describing a simple folding pathway (18). In FKBP, the structure of the crossing segments is determined by NOEs including Thr[14]-Ser[67], Gly[12]-Ser[67], Arg[13]-Ser[67], Pro[16]-Val[68], and Pro[16]-Leu[106]. There are van der Waals contacts between the side chains of Pro[16] and Leu[106], Val[68] and Leu[103], and Thr[14] and Val[68]. The hydrogen-bonding propensities of many residues in the crossing region (Pro[9], Asp[11], Thr[14], Met[66], Ser[67], and Val[68]) are satisfied through backbone-backbone and backbone–side chain interactions. All amide protons in the inner strand and two amide protons in the outer strand (Lys[17] and Gln[20]) exchange slowly when the protein is dissolved in D_2O; this result is indicative of hydrogen bonds stabilizing this topology.

In a preliminary study of the FKBP-FK506 and FKBP-rapamycin complexes we noted NOEs from the indole ring of Trp[59] and several other unidentified aromatic protons to the pipicolinyl ring of the bound drugs (13). Based on the solution conformation of FKBP, it was possible to define the binding region as an extensive aromatic cluster composed of Tyr[26], Phe[46], Phe[48], Trp[59], Tyr[82], and Phe[99]. These residues pack together with a number of aliphatic residues to form a large, well-defined hydrophobic core (Fig. 2D). Thus, FK506 and rapamycin bind in the hydrophobic pocket that consists of a twisted and curved antiparallel β-sheet platform with walls formed by an α helix and a long loop (Fig. 2B). The location and detailed structure of the binding site has been confirmed by the subsequent x-ray structure of the FKBP-FK506 complex (19). The architecture of the binding site, whose natural ligands are not known but may include peptides, is very different from those formed by β barrels in a number of proteins that bind hydrophobic ligands [such as P2 myelin protein (20) and bilin binding protein (21)]. However, although the overall structures are very different, the FKBP binding site has elements in common with that of the class I major histocompatibility complex (MHC) glycoprotein HLA-A2 (22), which has a flatter antiparallel β-sheet platform with walls formed by two long α helices. Peptide segments that form loops at the open end of the pocket, specifically, Asp[37] to Asn[43] and Gly[82] to Ile[90], are not well defined (see Fig. 2, A and B). The lack of long-range NOEs in both segments coupled with previous evidence of conformational exchange in the second (10) indicate that they may be flexible in solution. A comparison of ^{1}H and ^{15}N chemical shifts obtained from single-quantum coherence (SQC) spectra of [15]N-

Table 1. Structural and energetic statistics for FKBP. Structure determination was achieved with a simulated annealing protocol consisting of three stages: (i) a conformational search phase; (ii) an annealing phase; and (iii) a refinement phase (9, 30). Numbers in parentheses are the number of restraints in each class or the number of bonds, angles, and dihedrals in the structure geometry statistics. SA_i is the ith structure obtained by the protocol given above. The SA_i column gives the average and standard deviations for the indicated variables obtained from the 21 structures with the lowest empirical energies and residual violations of experimental restraints. $\langle SA \rangle_{ref}$ represents the average structure of SA_i least-square fit to each other including all atoms (except for residues 83 to 90) and refined with 1000 steps of steepest-descent energy minimization. The RMSDs are from the upper or lower bounds of the distance restraints; none of the structures showed deviations greater than 0.25 Å. Restraints were classified into the following categories based on strong, medium, and weak NOEs (11): backbone, 2.5 ± 0.5 Å, 2.75 ± 0.75 Å, 3.5 ± 1.5 Å; side chain, 2.5 ± 0.5 Å, 3.0 ± 1.0 Å, 3.5 ± 1.5 Å; 0.5 Å was added to the upper limits for distances involving methyl protons. Average RMSDs and standard deviations of the final structures SA_i against the refined average structure $\langle SA \rangle_{ref}$. For β sheet: backbone, 1.01 ± 0.16; all atoms, 1.92 ± 0.14. For α helix: backbone, 0.31 ± 0.07; all atoms, 1.05 ± 0.16. For all atoms except residues 83 to 90: backbone, 1.45 ± 0.20; all atoms, 2.49 ± 0.17.

Parameter		SA_i		$\langle SA \rangle_{ref}$
RMSDs from experimental distance restraints (Å)				
Total	(910)	0.024 ±	0.002	0.008
Peptide backbone restraints				
Intraresidue	(246)	0.011 ±	0.003	0.022
Interresidue sequential ($\lvert i-j \rvert = 1$)	(254)	0.024 ±	0.003	0.008
Interresidue short-range ($\lvert i-j \rvert \leq 5$)	(39)	0.041 ±	0.008	0.021
Interresidue long-range ($\lvert i-j \rvert > 5$)	(146)	0.031 ±	0.004	0.051
Side-chain restraints				
Intraresidue	(12)	0.008 ±	0.010	0.024
Interresidue sequential ($\lvert i-j \rvert = 1$)	(5)	0.012 ±	0.018	0.003
Interresidue short-range ($\lvert i-j \rvert \leq 5$)	(25)	0.018 ±	0.008	0.000
Interresidue long-range ($\lvert i-j \rvert > 5$)	(133)	0.023 ±	0.004	0.020
Hydrogen-bond restraints*	(50)	0.034 ±	0.008	0.037
Deviations from idealized geometry†				
Bonds (Å)	(1682)	0.013 ±	0.000	0.013
Angles (degrees)	(3047)	3.360 ±	0.064	3.240
Impropers (degrees)	(498)	0.460 ±	0.030	0.490
Potential energy statistics (kcal/mol)				
E_{total}		−2170.0	± 120	−2280.0
E_{bond}		47.8	± 3.1	49.9
E_{angle}		486.0	± 20	652.0
$E_{dihedral}$		512.0	± 18	532.0
$E_{improper}$		15.8	± 1.8	16.5
E_{vdw}		−336.0	± 15	−358.0
$E_{electrostatic}$		−2920.0	± 120	−3200.0
E_{chide}		5.6	± 1.7	5.9
E_{NOE}		27.0	± 3.9	22.3

*Backbone hydrogen bond restraints were assigned to ranges r_{NH-O} = 1.9 ± 0.5 Å and r_{N-O} = 2.8 ± 0.5 Å.   †Idealized geometries based on CHARMM parameters (31).

DOCKET ALARM

Explore Litigation Insights

Docket Alarm provides insights to develop a more informed litigation strategy and the peace of mind of knowing you're on top of things.

Real-Time Litigation Alerts

Keep your litigation team up-to-date with **real-time alerts** and advanced team management tools built for the enterprise, all while greatly reducing PACER spend.

Our comprehensive service means we can handle Federal, State, and Administrative courts across the country.

Advanced Docket Research

With over 230 million records, Docket Alarm's cloud-native docket research platform finds what other services can't. Coverage includes Federal, State, plus PTAB, TTAB, ITC and NLRB decisions, all in one place.

Identify arguments that have been successful in the past with full text, pinpoint searching. Link to case law cited within any court document via Fastcase.

Analytics At Your Fingertips

Learn what happened the last time a particular judge, opposing counsel or company faced cases similar to yours.

Advanced out-of-the-box PTAB and TTAB analytics are always at your fingertips.

API

Docket Alarm offers a powerful API (application programming interface) to developers that want to integrate case filings into their apps.

LAW FIRMS
Build custom dashboards for your attorneys and clients with live data direct from the court.

Automate many repetitive legal tasks like conflict checks, document management, and marketing.

FINANCIAL INSTITUTIONS
Litigation and bankruptcy checks for companies and debtors.

E-DISCOVERY AND LEGAL VENDORS
Sync your system to PACER to automate legal marketing.

fastcase
Smarter legal research.